

Full length article

Tooth structure, mechanical properties, and diet specialization of Piranha and Pacu (Serrasalminae): A comparative study

Audrey Velasco-Hogan^a, Wei Huang^b, Carlos Serrano^c, David Kisailus^b,
Marc A. Meyers^{a,c,d,*}

^a Materials Science and Engineering Program, University of California, San Diego, United States

^b Department of Materials Science and Engineering, University of California, Irvine, United States

^c Department of Mechanical and Aerospace Engineering, University of California, San Diego, United States

^d Department of Nanoengineering, University of California, San Diego, United States

ARTICLE INFO

Article history:

Received 21 April 2021

Revised 9 August 2021

Accepted 17 August 2021

Available online 21 August 2021

Keywords:

Micro-CT

Nanoindentation

Finite element analysis

Bioinspiration

Interface

ABSTRACT

The relationship between diet, bite performance, and tooth structure is a topic of common interest for ecologists, biologists, materials scientists, and engineers. The highly specialized group of biters found in Serrasalminae offers a unique opportunity to explore their functional diversity. Surprisingly, the piranha, whose teeth have a predominantly cutting function and whose main diet is soft flesh, is capable of exerting a greater bite force than a similarly sized pacu, who feeds on a hard durophagous diet. Herein, we expand our understanding of diet specialization in the Serrasalminae family by investigating the influence of elemental composition and hierarchical structure on the local mechanical properties, stress distribution, and deformation mechanics of teeth from piranha (*Pygocentrus nattereri*) and pacu (*Colossoma macropomum*). Microscopic and spectroscopic analyses combined with nanoindentation and finite element simulations are used to probe the hierarchical features to uncover the structure-property relationships in piranha and pacu teeth. We show that the pacu teeth support a durophagous diet through its broad cusped-shaped teeth, thicker-irregular enameloid, interlocking interface of the dentin-enameloid junction, and increased hardness of the cuticle layer due to the larger concentrations of iron present. Comparatively, the piranha teeth are well suited for piercing due to their conical-shape which we report as having the greatest stiffness at the tip and evenly distributed enameloid.

Statement of significance

The hierarchical structure and local mechanical properties of the piranha and pacu teeth are characterized and related to their feeding habits. Finite element models of the anterior teeth are generated to map local stress distribution under compressive loading. Bioinspired designs from the DEJ interface are developed and 3D printed. The pacu teeth are hierarchically structured and have local mechanical properties more suitable to a durophagous diet than the piranha. The findings here can provide insight into the design and fabrication of layered materials with suture interfaces for applications that require compressive loading conditions.

© 2021 Acta Materialia Inc. Published by Elsevier Ltd. All rights reserved.

1. Introduction

The dynamics of prey consumption and processing are strongly linked with tooth morphology and function. Teeth have long played a key role in assessing dietary adaptation in mammals as highlighted by 18th century naturalist Georges Cuvier: “show me your teeth and I will tell you who you are” [1–4]. However, there

remains little investigation into the hierarchical structure, property, and function relationships of teleost fishes, especially of those belonging to families of highly specialized biters. Teeth, being composites of hydroxyapatite and collagen, form complex structures at various orders of hierarchy ranging from the nano- to macro-scale as a result of their bottom-up growth and self-assembly from the molecular level. This hierarchical organization and the respective local material properties ultimately determine the overall mechanical properties and performance of the tooth. This information is important in establishing relationships between structural varia-

* Corresponding author.

E-mail address: mameyers@ucsd.edu (M.A. Meyers).

tion, mechanical performance, and diet specialization among understudied teeth such as those of teleost fishes.

Teeth are a crucial evolutionary adaptation to vertebrates allowing for diet specialization [5–9]. Despite the vast range of morphological differences at the macro-scale including size, shape (e.g., conical, pointed, flat, cusps, broad, or curved), and number, teeth have a highly-conserved structure at the meso-scale which consists of three layers: (1) enamel/enameloid, (2) dentin, and (3) pulp in order from outer-to-inner respectively [10,11]. The enamel and enameloid are highly mineralized tissues which covers the functional surface of the tooth providing wear-resistance and hardness [12]. Enamel is typically found in mammalian-vertebrates and enameloid in non-mammalian vertebrates. Enamel and enameloid have similar compositions, having a high mineral content (~95 vol% of hydroxyapatite ($\text{Ca}_5(\text{PO}_4)_3\text{OH}$)) which forms highly crystalline hexagonal rods. In both enamel and enameloid, hydroxyapatite is known to contain impurities including carbonate, magnesium, and sodium. The enameloid of actinopterygians (bony fishes) occurs in two regions: (1) cap enameloid at the tip of the tooth, and (2) collar enameloid on the shaft of the tooth [12,13]. The dentin layer is much less mineralized (~45 vol%) than the enamel/enameloid and is formed by odontoblasts [13,14]. The dentin layer is characterized by a tubule structure which results from the formative tracks of odontoblastic cells. Finally, the pulp is the central part of the tooth which is non-mineralized and contains blood vessels, connective tissue, and nerves [14].

Teleosts are known to employ three primary feeding modes involved in prey-resource capture: (1) ram-feeding, where the fish propels its body and engulfs its prey with its large agape mouth [15,16], (2) suction-feeding, where prey is drawn into the mouth driven by a negative pressure in the buccal cavity [17,18], and (3) manipulation-feeding or biters which crush, slice, or tear prey with a robust oral jaw system [19,20]. Of the three feeding modes, manipulation-feeding or biters require high mechanical advantage for jaw-closing, a large adductor mandibula for powerful force-generating capacity, and functional teeth which act as cutting/crushing tools [20]. Unlike many families in the teleost class, Serrasalminae, a monophyletic family of South American freshwater fishes, are exclusively manipulative feeders, also referred to as biters, and thus represent a unique opportunity in which to investigate the relationships between diet, tooth hierarchical structure, composition, and mechanical properties.

Serrasalminae contains highly specialized biting fishes categorized by three subclades: piranha-clade, pacu-clade, and *Myleus*-clade. These subclades are distinguished by their distinct feeding habits and remarkable dentition [21]. The work reported here will focus on the piranha- and pacu-clade. Piranha typically have triangular-shaped, tricuspid, and serrated teeth found within a single row. The teeth interlock with their adjacent neighbors' lateral cusps creating a unified unit that regenerates as a row simultaneously [22]. This interlocking mechanism is described as a “peg and socket” where the adjacent lateral cusp inserts within its neighbors' cusp acting as a cap. It is hypothesized that the interdigitation helps to distribute the stress that acts on a few teeth across the entire row during mastication [22]. Piranha also possess heterodont dentition where their tooth morphology is distinct depending on location within the jaw [22]. *Serrasalmus rhombeus*, commonly known as the Black piranha, has been shown to have the most powerful bite force relative to its size with a maximum recorded bite of 320 N for a 1.1 kg specimen [23]. This is primarily attributed to its large adductor mandibulae complex which makes up over 2% of its total body mass [23]. The piranha is famously known for being piscivory and carnivorous [24,25] as it relies on its sharp pointed teeth to slice and tear through fleshy meat [26,27].

In contrast, the pacu is herbivorous feeding on hard-shelled fruits, seeds, and leaves [28,29]. The pacu are known to have one

and/or two rows of broad incisiform-to-molariform teeth depending on location within the jaw [27,30,31]. Thus, pacu teeth are highly heterodont. Their teeth have large occlusal surface areas with conical projections. Similar to piranhas, the teeth of the pacu support their adjacent neighbors and regenerate as a row simultaneously [22]. However, the interlocking mechanism in the pacu teeth is much more subtle and does not fully interdigitate and can be described as a “buttress” where the adjacent lateral sides slightly overlap providing support [22]. This buttress-style interlocking similarly found in the anterior teeth of the durophagous horn-shark (*Heterodontus*) [32]. The pacu uses its incisiform and molariform teeth for masticating hard substances [29].

These known differences in diet between the piranha and pacu have led to the proposal that pacus have larger jaw muscles and bite forces needed for crushing hard substances when compared to their carnivorous counterparts. This prediction has been demonstrated by studies in which species with a more durophagous diet typically are capable of exerting larger bite forces [33–38]. Recently, this hypothesis in relation to the bite force capacities between piranhas and pacus has been disproven by Huby et al. [39] in a comprehensive study dedicated to characterizing the oral jaw system in Serrasalminae fishes. The resulting study showed that in vivo and theoretical size-removed bite forces are significantly greater in piranhas due to their proportionally larger adductor mandibulae muscle [39]. It was found that the mass of the adductor mandibulae muscle is four times greater in the piranha-clade than the pacu-clade with respect to size [39]. However, this proportionality is not distributed equally among the three main muscle subdivisions. The pars rictalis is four times larger in the pacu-clade, the pars malaris is twice as large in the piranha-clade, while the pars stegalis is equivalent in both [39]. These relative size differences in the subdivision of the adductor mandibulae have important consequences on how the bite force is distributed across the jaw. This suggests that the pacu-clade transmits relatively more force to the most anterior teeth in the lower jaw, while the piranha-clade transmits relatively more force to the most posterior teeth in the lower jaw [39]. While general trends point towards a relationship between durophagy and greater bite forces, this study is not the only one to suggest that durophagy can be achieved despite a respectively low bite force [40]. We suggest that the mechanical properties of the molariform teeth of the pacu, as dictated by their hierarchical structuring, allow for the pacu to effectively facilitate consumption of a specialized durophagous diet.

A recent study by Delaunois et al. [41] describes the microstructure and composition of the enameloid in piranha, *Pygocentrus nattereri*, and pacu, *Piaractus brachypomus*. It was found that the enameloid, in both species, has three distinctive regions: (1) cuticle, the outermost layer, (2) outer enameloid described by a parallel-structured layer, and (3) inner enameloid, described by a woven layer, which highlights the preservation of histological traits in the tooth structure of Serrasalminae. However, there were differences in cuticle thickness between the two species which can be related to their distinct diets, herbivorous versus carnivorous. It was found that the pacu has a thicker cuticle (1.90 μm) compared to the piranha cuticle (0.79 μm) [41]. Additionally, the pacu cuticle has a higher concentration of iron which is known to increase hardness and stiffness [41,42]. Therefore, it is suggested that the thicker pacu cuticle can help reduce detrimental wear resistance as an adaptation to its durophagous diet. Despite the greater presence of iron in the pacu teeth, the piranha teeth were shown to be more mineralized [41].

This study highlights the important microstructural and compositional variations between two closely related species with distinct feeding habits and warrants exploration into their local mechanical properties via nanoindentation. While nanoindentation has been performed on piranha teeth by Chen et al. [43] this study

only examined the transverse cross section, despite the fact that teeth have consistently shown to have highly anisotropic properties and nanoindentation of pacu teeth is absent in the literature [44–47]. Our work on characterization of the mechanical properties of the piranha and pacu teeth will fill this void.

2. Materials and methods

2.1. Specimens

Three adult piranha (*Pygocentrus nattereri*) and three adult pacu (*Colossoma macropomum*) specimens were purchased from local fish markets in Brazil already deceased. Specimens were transported overnight packed in ice. Upon retrieval specimens' standard lengths were recorded and their intact skulls preserved and placed in a $-20\text{ }^{\circ}\text{C}$ freezer until use. Specimens were hydrated in Hank's balanced salt solution (Thermo Fisher Scientific) before jaw muscle dissection. The lower jaws were removed and only the most anterior teeth were examined further. The anterior teeth were studied as evidence from Huby et al. [39] which suggests that these are the dominant teeth used by the pacu for crushing and their muscle and jaw configuration allows the pacu to have superior mechanical advantage towards the anterior teeth. The anterior teeth were sonicated to remove debris and critically dried using a critical point dryer (Autosamdri-815, Tousimis, Rockville, MD, USA). They were stored at room temperature and then embedded in epoxy for further sectioning and polishing. The specimens used were not stored in formalin at any time.

2.2. Quasi-static compression

Four palm seeds (*Jubaea chilensis*) were tested in quasi-static compression using a mechanical testing machine, Instron 3367 load frame (Instron, High Wycombe, United Kingdom) to determine the forces required to initiate and propagate a crack under compression. A strain rate of 10^{-2} s^{-1} was used. The force-displacement curves and failure mechanisms were highly repeatable for all nut samples tested.

Four piranha teeth and four pacu teeth were superglued to screws at the base of the tooth that could then be attached to a mechanical testing machine that was used to penetrate into the flesh of a fresh tilapia (*Oreochromis aureus*) purchased at the local market. Samples were compressed at a rate of 2 mm/s. This velocity was chosen as it the fastest velocity that the Instron tester was able to reach with appropriate results in attempts to reflect biting velocity. The fish was unmodified with its scales and skeleton still attached. All tests occurred in the epaxial muscle above the lateral line and below the dorsal fin. The tilapia was sufficiently large that indents were able to be performed in the same approximate location. The force-displacement curves and failure mechanisms were highly repeatable for both the piranha and pacu teeth.

2.3. Embedding, grinding, and polishing

Anterior mandibular teeth were extracted and embedded in Epo-Tek 301 epoxy and allowed to polymerize overnight at $25\text{ }^{\circ}\text{C}$. Samples were then ground and polished in either the longitudinal (coronal) or transverse (axial plane). The surface was ground using subsequently finer grits of Buehler SiC grinding paper (320, 600, 800, & 1200 grit). Ground samples were polished using $3\text{ }\mu\text{m}$ and $1.0\text{ }\mu\text{m}$ polycrystalline aqueous diamond polishing suspensions on a Buehler Trident polishing cloth. Samples were rinsed with water and dried under flowing argon gas.

2.4. Acid etching

Freshly polished, epoxy-embedded samples were etched for 1 min at $25\text{ }^{\circ}\text{C}$ in 30% HCl. Acid etching was used to reveal microstructural patterns in the enameloid and dentin. Upon grinding and polishing, mineral can fill the voids in the dentin tubules and obscure microstructural details.

2.5. Scanning electron microscopy

For SEM imaging, samples were sputter coated with iridium at $85\text{ }\mu\text{A}$ for 8 seconds at a deposition pressure of 10^{-2} Pa of Ar gas to reduce charging using a sputter coater (Emitech K575X, Quorum Technologies Ltd, East Sussex, UK). Micrographs were collected using FEI Quanta 250 operating at 5 kV with a spot size of 3 in high vacuum mode.

2.6. Energy dispersive spectroscopy and X-ray mapping (EDS)

Polished and sputter coated samples (not acid-etched) were used to collect standardless quantitative elemental analysis using the FEI Quanta 250 with the Pathfinder X-ray microanalysis software (Thermo Fisher Scientific) and a Thermo Scientific™ UltraDry EDS Detector Model: INTX-10P-A. An operating voltage of 30 kV with a spot size of 5 was used. X-ray maps were collected at 512×512 pixel with an acquisition time of 50 s. EDS was performed in both the transverse (axial) and longitudinal (coronal) planes.

2.7. Micro-computed X-ray tomography

Four anterior mandibular teeth (two pacu and two piranha) were imaged (Xradia 510 Versa, ZEISS, Jena, Germany) with a voxel size of ranging from $4.129\text{--}9.579\text{ }\mu\text{m}$ (depending on tooth size) and an accelerating voltage of 80 kV. The images were processed using Amira® software (FEI, Oregon, USA).

2.8. Nanoindentation

High-resolution nanoindentation was performed to ascertain the regional hardness and modulus of both anterior teeth. Nanoindentation experiments were conducted using a TI-950 TriboIndenter (Hysitron, USA) with a low-load transducer. Samples were tested using a diamond cube corner probe. All maps featured an array of indents with a spacing of $10\text{ }\mu\text{m}$ in the horizontal and vertical directions. Indents were controlled in displacement between 200 nm and 500 nm. Partial unloading tests were first conducted in each sample to determine the appropriate minimum depth to overcome surface roughness. A trapezoidal load function consisting of a 5 s load, 2 s hold, and 5 s unload was used for all mapping experiments. Indents were performed on both longitudinal (coronal) and transverse (axial) cross sections of polished sections. The analysis plane was chosen such that the midplane of the tooth was exposed and the enameloid, DEJ, and dentin could be mapped. As a consequence of indenting on the midplane, only the coronal section allowed for indentation of the cuticle layer as the cuticle layer decreases in thickness away from the tip of the tooth.

2.9. Modeling

Individual teeth (most anterior) from both pacu and piranha were isolated and subjected to x-ray microscopy to obtain 3D meshes. The image slices obtained from micro-computed x-ray tomography were rendered and segmented using the threshold tool in Amira® software (FEI, Oregon, USA) and outputted as STL files. These files were then used in Meshmixer (Autodesk) to simplify

and reduce cracks and holes in the mesh. The mesh was then finalized in Autodesk Fusion 360 and converted into a .SAT file that could be readily inputted into Abaqus.

Numerical simulations on the most anterior teeth of the piranha and pacu were performed using finite element software Abaqus (v.6.14). The models were separated into two mechanically distinct parts (dentin and enameloid). Dentin and enameloid phases were modeled as linear elastic materials with different values of modulus obtained directly from the nanoindentation experiments: i) the enameloid with two elastic moduli (80 GPa for the piranha and 75 GPa for the pacu), and ii) the dentin with two elastic moduli (23 GPa for the piranha and 22 GPa for the pacu). The Poisson's ratio for both layers was assumed to be 0.3. All nodes in the bottom surface of the piranha tooth were fixed in all directions, while all nodes on the exposed lingual surface of the pacu tooth were fixed in all directions (Figure S3). A uniaxial pressure was applied to the surface of the tip of each tooth that corresponds to a 15 N load. The model was fully meshed using C3D10 elements (10-node quadratic tetrahedron elements) and a mesh convergence study was carried out. Nonlinear effects were excluded. The interface between the enameloid and dentin was assumed to be perfectly bonded.

The bioinspired structures were subjected to a similar protocol. The prototypes are inspired by the flat and suture interfaces of the DEJ found in the piranha and pacu respectively. The prototypes were drawn using Autodesk Fusion 360 allowing for them to be directly imported into Abaqus. The models were separated into two mechanically distinct parts (Veroclear and Flex). The phases were modeled as linear elastic materials. All nodes in the bottom surface of each prototype were fixed in all directions. A uniaxial pressure was applied on the top surface to compress the prototypes. The interface between the two layers was assumed to be perfectly bonded. The model was fully meshed using hexahedral elements; a mesh convergence study was carried out. Nonlinear effects were excluded.

2.10. Mechanical testing of bioinspired prototypes

The bioinspired prototypes with differing interfaces (flat vs interdigitating) were designed in Autodesk Fusion 360 and printed using the Objet360 Connex3 (Stratasys, Poway, CA USA) with UV-cured material Veroclear (representing the enameloid) and Flex (representing the dentin). After printing, the support material was physically removed. The prototypes were designed as cubes with a side length of 20 mm. Both prototypes have equal masses as material composition was preserved.

Quasi-static compression tests were performed using a mechanical testing machine, Instron 3367 load frame (Instron, High Wycombe, United Kingdom). Three samples of each prototype were tested (flat interface vs triangular suture interface). A load was applied with a constant speed of 0.20 mm/s. The force-displacement curves and failure mechanisms were highly repeatable and consistent for all samples.

2.11. Statistical information

Mann-Whitney test was performed with a 95% confidence interval using GraphPad Prism 9.

3. Results and discussion

3.1. Theoretical anterior bite force and allometry

In order to better understand how the piranha and pacu teeth distribute stress during biting, the anterior bite forces are calculated. The theoretical bite force of both the piranha and pacu can be estimated from the geometry of the maxilla and the size of the adductor mandibular muscles using an approach developed by Westneat [48] and adapted by Meyers et al. [49] In this adaptation, the closing of the lower jaw can be modeled as a third-order lever. There are three major subdivisions of the adductor mandibular muscle that are responsible for closing, referred to as A1, A2, and A3. The major force generators in the jaw are the A2 and A3 subdivisions. Measured values of the angles ($\alpha_1, \alpha_2,$ and α_3), segments ($d_1, d_2, d_3,$ and d_o), and maximum cross sections of the three-muscle groups are used to calculate the forces (Fig. 1). The equations of equilibrium are:

$$\sum ME = F_{A1} \sin(\alpha_1)d_1 + F_{A2} \sin(\alpha_2)d_2 + F_{A3} \sin(\alpha_3)d_3 - F_{output}d_o = 0 \tag{1}$$

The force of the muscles ($F_{A1}, F_{A2},$ and F_{A3}) can be approximated knowing the cross-sectional area and the muscle stress of $200 \text{ kN}\cdot\text{m}^{-2}$ which is the highest range for red muscles as indicated by Westneat [48]. The segments (d_1, d_2, d_3) are the lengths between the fulcrum and the attachment point for each muscle and d_o is the length from the fulcrum to the most anterior tooth tip.

The theoretical maximum anterior bite force for the piranha is greater than the pacu for the same standard length (Fig. 2A). This agrees with prior studies who measured in vivo and theoretical bite forces [39]. Our bite forces for the piranha ranged from ~20 to 80 N and for the pacu ~6 to 72 N with dependence on specimen

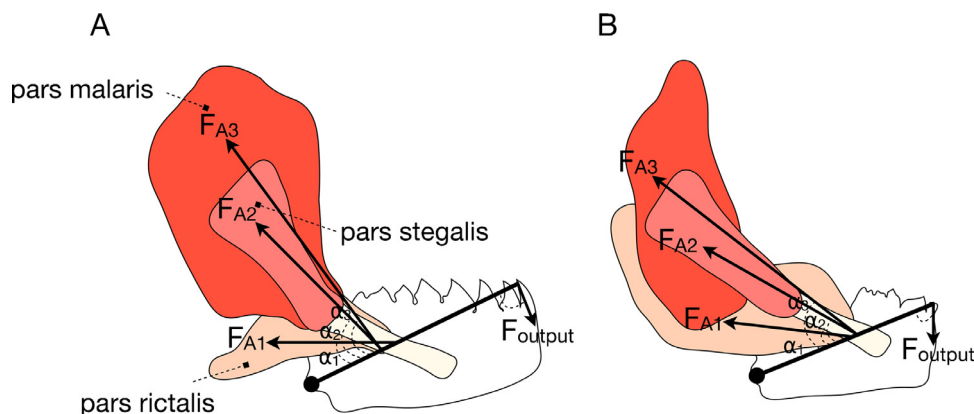


Fig. 1. Schematic of the medial cross section of the adductor mandibular muscle and its three main subdivisions in (A) *Pygocentrus nattereri* (piranha) and (B) *Collossoma Macropomum* (pacu). $F_{A1}, F_{A2},$ and F_{A3} correspond to the resultant forces of the three adductor mandibular subdivisions: pars rictalis, pars stegalis, and pars malaris respectively. The angles that each subdivision make in contact with the jaw are labeled as $\alpha_1, \alpha_2,$ and α_3 . The bite force is defined as F_{output} .

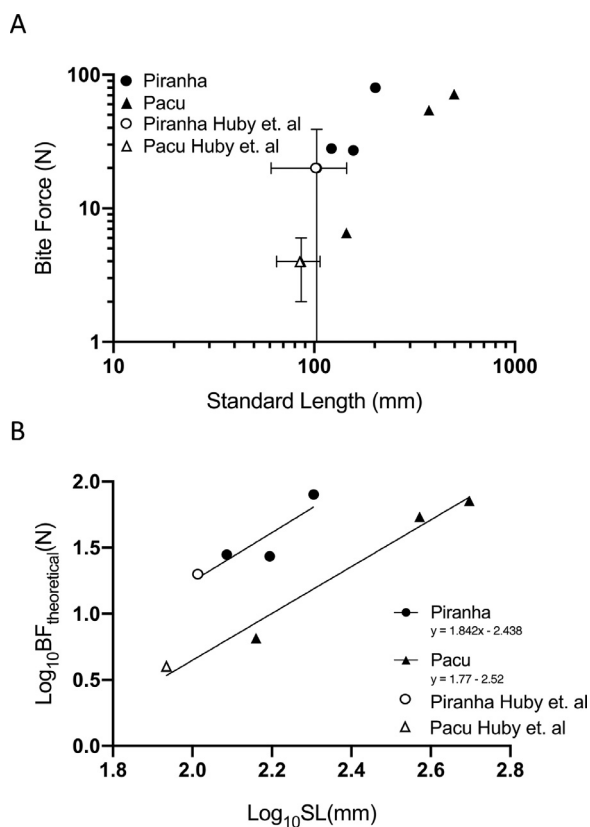


Fig. 2. Theoretical bite forces of *Pygocentrus nattereri* (piranha) and *Colossoma Macropomum* (pacu) specimens with addition of the average values obtained by Huby et al. [39] which show how bite force scales with the standard length of the fish. A) Theoretical bite force as a function of the to the standard length of piranha and pacu which includes the average data collected from Huby et al. [39]. This shows a bite force for the piranha which ranges from ~1–80 N and ~4–72 N for the pacu. Despite the larger size of the pacu, the piranha still manages a greater bite force. B) Log transformed theoretical bite force and standard length which demonstrates a positive allometric relationship.

standard length (SL). This is consistent with Huby et al. [39] who calculated values of ~1 to 42 N for the piranha and ~1 to 17 N for the pacu [39] using similarly sized fishes and with respect to SL. Even for similarly sized fish, the piranha exerts a greater bite force than the pacu (Fig. 2). This difference is attributed to the piranha's larger adductor muscle with respect to a similarly sized pacu. The piranha's adductor mandibula is proportionally larger than the pacu's which accounts for the greater anterior bite force. While there is a trend for the piranha to have a greater-size removed bite force than the pacu, our data does show that there is not a significant difference in the anterior theoretical bite force between the piranha (mdn = 28 N) and the pacu (mdn = 54 N) groups ($U = 4$; $P > 0.999$) when using a non-parametric Mann-Whitney U test. This could be a result of small sample size $n = 3$.

Additionally, we report both theoretical bite forces scale allometrically with the standard length of the fish with allometric constants of 1.842 and 1.77 for the piranha and pacu, respectively (Fig. 2B). Indeed, these allometric constants are close to the expected value of 2.0 [50]. Despite the piranha having a greater size-removed bite force, it is noted that the pacu can grow to a significantly larger size than the piranha [31]. Therefore, it is possible for large pacu to exert a considerable bite force much greater than a piranha. This can have consequences for feeding performance and ontogeny similar to the sheephead (*Archosargus probatocephalus*)

whose diet changes with growth; feeding on soft invertebrates as a juvenile and then hard-shelled prey when matured [51].

We explored the forces necessary for consumption based on typical food sources for the piranha and pacu. The palm seed fruit is a common food source for the pacu and is used here to indicate the forces required to crack open hard-shelled fruits. When analyzed under compression it was found to require ~8 N to initiate a crack and ~25–35 N to propagate the crack (Fig. 3A). In comparison to the theoretical anterior bite forces, the pacu can reach ~8 N and induce a crack in this example of a hard-shelled fruit if the pacu is sufficiently large (Fig. 3A). While crack propagation, from this experiment, requires much larger species (SL > 130 mm), this value can be considered as an over-estimation as it was an example of a singular bite. In reality, multiple teeth may be used. During mastication and with repeated bites the pacu can easily damage the nut by fatigue which would require smaller forces over several cycles. This fast, repeated jaw adduction is used by the durophagous bonnethead shark when crushing hard-shelled prey [40].

To better understand the forces required for a carnivorous diet, piranha and pacu teeth were attached to a testing machine and advanced into the meat of a whole fish. Fig. 3B shows the load-penetration curves for both piranha and pacu teeth. The piranha teeth easily penetrate the scales and into the flesh at ~2–5 N as indicated by the rapid drop in force (highlighted in orange). The pacu teeth are unable to pierce the meat and instead cause a flattening effect. This provides evidence as to how the conically-shaped teeth are designed for piercing while the cusped-teeth of the pacu are more suitable for crushing. This has been shown to occur in shark teeth where broader triangular teeth are less efficient at puncturing when compared to narrower teeth [52]. In another similarity to sharks, the puncture load of bony fishes is surprisingly low (as low as <1 N) in contrast to their remarkably high bite forces [52] which is comparable to our finding of the piranha teeth. The estimation of the bite forces required for feeding is necessary to better understand the stress distribution and the load carried by individual teeth. The values obtained here will serve as a guide to what forces will be used for the finite element analysis.

3.2. Tooth morphology, enameloid thickness, and distribution

The anterior mandibular teeth of the piranha and pacu are strikingly different in shape and morphology. The piranha tooth is prominently tricuspid, has a conically-shaped tip, and a wide base, making it effective at piercing and slicing (Fig. 4A). The pacu tooth, on the other hand, has a broadly shaped occlusal surface with a projecting cutting ridge which is advantageous for crushing and grinding (Fig. 4D). In addition to their general morphological differences, both teeth have differences in enameloid thickness and distribution. It is widely accepted that enamel shape and thickness are highly related to diet. The consumption of hard-objects such as seeds and nuts is correlated with an increase in enamel thickness for mammals [53]. From the micro-computed tomography images, it can be seen that the molariform teeth of the pacu have thicker enameloid when compared to the piranha. The pacu enameloid is thickest on the cusps (1.5 ± 0.7 mm), while the piranha enameloid is more evenly distributed across the tooth (0.5 ± 0.3 mm) (Fig. 4). For both teeth, there is a gradient in enameloid distribution which increases from the base towards the tip. This gradient is most likely a consequence of the growth and development of the enameloid layer but has desirable implications for their respective mechanical performances. Enameloid being a hard, stiff, and wear resistant material provides rigidity to the tips of both teeth which enables effective puncturing and crushing. While the enameloid is rather evenly distributed in the piranha (Fig. 4B and C), for

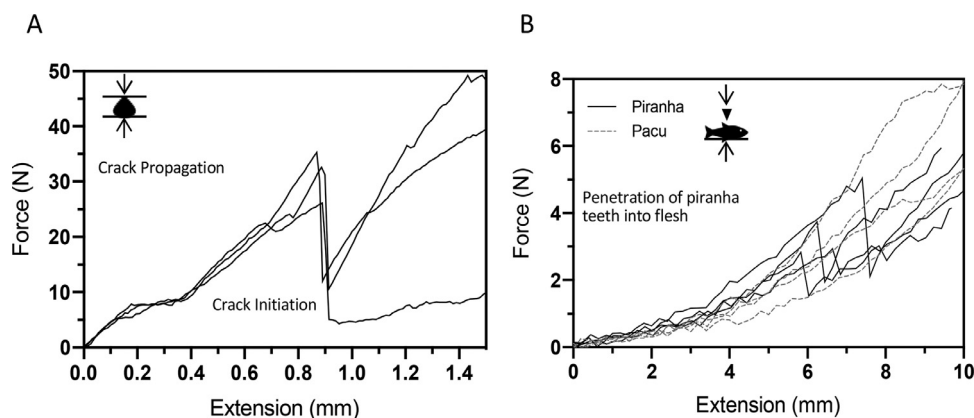


Fig. 3. Forces required for feeding with respect to relative diets. A) Compression testing of palm seeds. Palm seeds are a known food source of the pacu. They require ~7 N to initiate a crack (green) and ~30 N to propagate the crack (blue). B) Force-penetration curves into fish meat by individual piranha and pacu teeth. It requires ~2–5 N for the piranha tooth to penetrate the scale surface into the flesh. The pacu teeth are not able to penetrate and instead compress and flatten the meat.

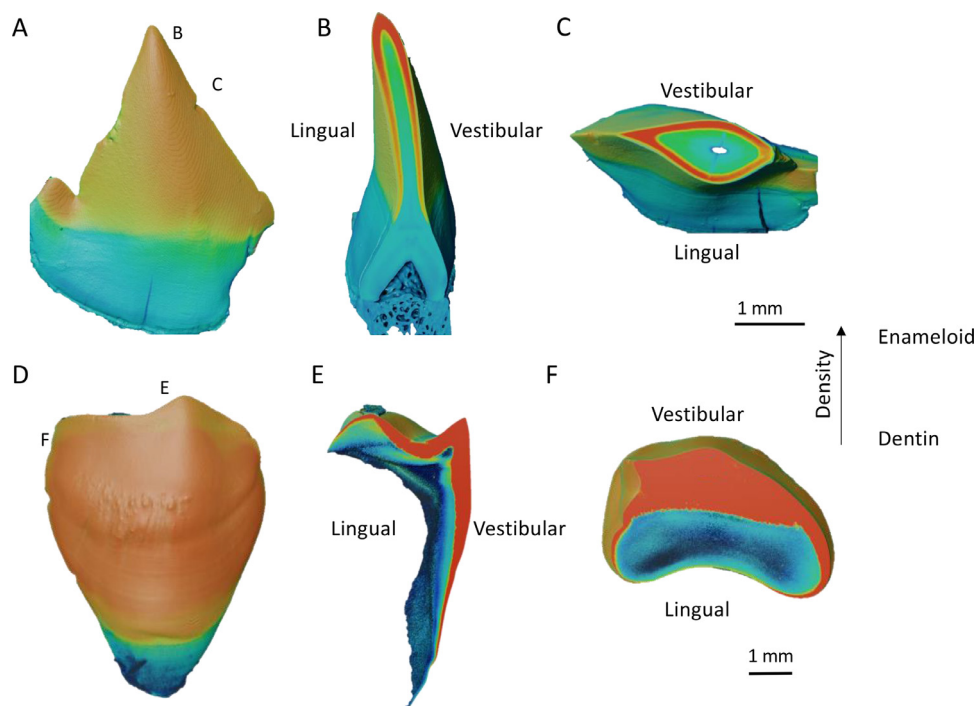


Fig. 4. Micro-computed tomography images of anterior *Pogonias cromis* (piranha) and *Colossoma Macropomum* (pacu) teeth which are pseudo-colored. The coloration is a relative density map where the hotter colors correspond to a denser and more mineralized phase (enameloid) and the cooler colors correspond to a less dense and less mineralized phase (dentin); in the case of the piranha the bone is shown in blue as well. A) Vestibular surface of the piranha tooth. B) Longitudinal cross section of the piranha tooth. C) Transverse cross section of the piranha tooth. D) Vestibular surface of the pacu tooth. E) Longitudinal cross section of the pacu tooth. F) Transverse cross section of the pacu tooth.

the pacu, the enameloid is strongly concentrated on the vestibular surface and protrudes to a maximum thickness of ~2 mm while being marginally thin on the lingual surface (Fig. 4E and F). This large concentration of thick enameloid provides a robust ledge for crushing and grinding. These differences in enameloid distribution are related to how the teeth are attached to the jaw.

In addition to their differences in general morphology and enameloid thickness, both teeth are attached to the mandible at different surfaces which has implications for how the load is distributed during mastication. The piranha tooth is embedded into the bone at its base, allowing for both the lingual and vestibular surfaces to be exposed to the environment (Fig. 4B). This enables a greater penetration and piercing action of the tooth. However, the pacu tooth does not have a defined base and is instead embedded into the mandible, predominantly along the lingual surface, leaving

only the vestibular and occlusal surfaces exposed (Fig. 4E and Figure S1). Unlike the piranha, the pacu tooth is more anchored into the jaw, allowing for greater stabilization during compression and translation of mastication forces into the mandible. Thus, the thickness of the occlusal surface that is exposed above the mandible is minimal, which supports its primarily crushing mode.

3.4. Microstructure characterization of enameloid and dentin layers

3.4.1. Enameloid

The enameloid is highly mineralized and can be decomposed into two layers in both the piranha and pacu: (1) inner-enameloid (IE), where there is a high degree of interwoven HAP-mineralized collagen fibers, and (2) outer-enameloid (OE), which is defined by aligned regions perpendicular to the surface (vertical lines in

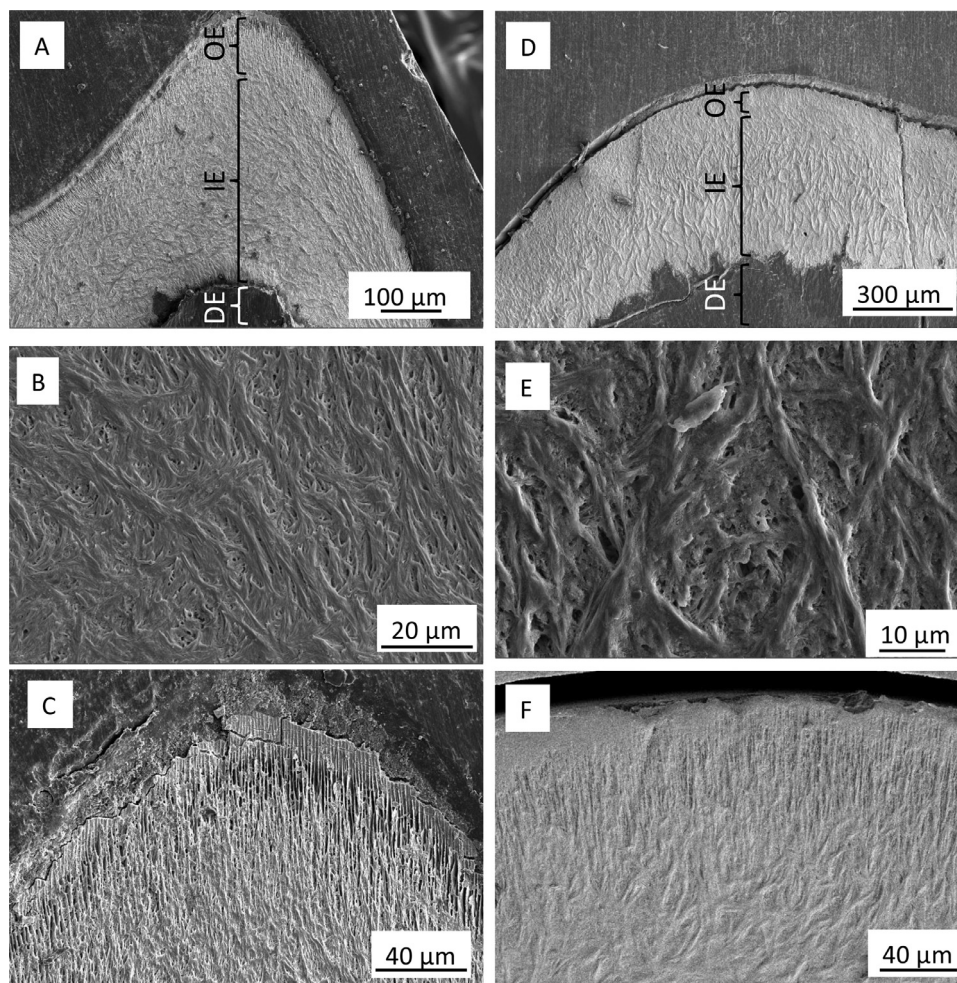


Fig. 5. SEM images of acid-etched enameloid of *Pygocentrus nattereri* (piranha) and *Colossoma Macropomum* (pacu) which shows the following layers: outer enameloid (OE), inner enameloid (IE), and dentin (DE). A) Longitudinal cross section of a piranha tooth showing the three layers: OE, IE, and DE. B) Magnification of the IE from the piranha tooth showing the woven fibrous network. C) Magnification of the OE of the piranha tooth showing the parallel oriented rods that are perpendicular to the surface. D) Longitudinal cross section of a pacu tooth showing the three layers: OE, IE, and DE. E) Magnification of the IE from the pacu tooth showing the woven fibrous network. F) Magnification of the OE showing the parallel orientated rods.

Fig. 5). Demineralization with HCl was used to reveal the microstructure which can be concealed by amorphous regions. The inner-enameloid in both piranha and pacu shows no significant differences in the organization, size, or dispersion of the mineral-coated collagen fibers (Figs. 4B and E). The thickness of the fibers area $2.5 \pm 0.8 \mu\text{m}$ in the piranha and $2.5 \pm 0.8 \mu\text{m}$ (mean \pm standard deviation) in the pacu and the angle between fibers which cross over each other are $56^\circ \pm 17^\circ$ and $56^\circ \pm 11^\circ$ respectively. These similarities are attributed to equivalences in tissue development. The imbrication found in the IE has the potential capability of arresting and deterring cracks from propagating through the enameloid and may act as a toughening mechanism for the inherently brittle material [54]. The OE responded differently to the demineralization process in both teeth. The OE of the piranha teeth show a higher degree of demineralization when compared to the OE of the pacu teeth (Figs. 4C and F). This is possibly explained by the differences in iron concentration. As shown by Delaunois et al. [41] and corroborated in Section 3.5, the pacu teeth have a greater concentration of iron which has been shown to improve resistance against acid attack in mammalian teeth [42].

When compared to mammalian enamel, the enameloid found in the piranha and pacu does not form well-ordered prisms and thus lacks defined prism interfaces [55]. The interfaces between enamel prisms in mammals are inherently weak and offer paths

for crack propagation which is critical for their high damage tolerance [55]. The weak interface allows for cracks to preferentially grow between prisms rather than catastrophically through the bulk material allowing for control and minimization of damage [55]. This difference in enamel and enameloid can possibly stem from differences in ontogeny as enamel is secreted by the inner-dentin epithelium and enameloid is formed by both the inner-dentin epithelium and the ectomesenchymal cells of the dentin papilla; and composition of the organic matrix where enamel is exclusively composed of ectodermal proteins and enameloid has both ectodermal proteins and mesodermal collagen fibers [56,57]. Additionally, most mammals are typically diphyodont (only producing two sets of teeth) and the piranha and pacu are polyphyodont (producing many sets of teeth) which may reduce the need for this element of dental resiliency.

3.4.2. Dentin

The dentin layers are similar in both species and are characterized by the presence of tubules (Fig. 6). The tubules are generally cylindrical in shape, but depending on the cross section angle can appear elliptical if viewed obliquely. The average radius of the tubules in the piranha dentin was found to be $0.69 \mu\text{m}$ which is comparable to the pacu dentin ($0.71 \mu\text{m}$). Both dentin layers ex-

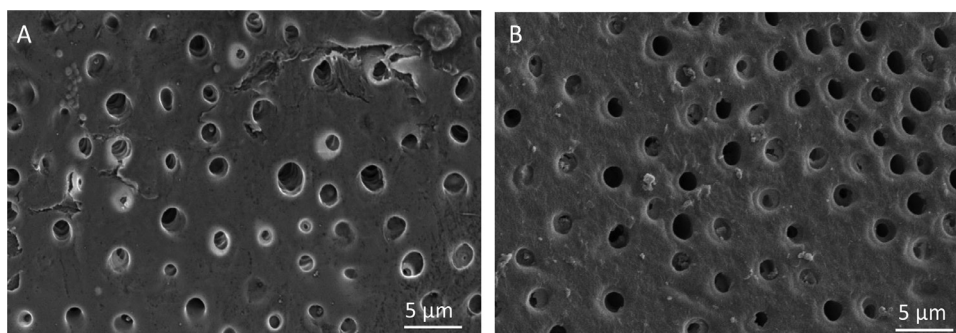


Fig. 6. SEM images of transverse cross sections showing the tubule structure in the dentin layer. A) Piranha tubular dentin. B) Pacu tubular dentin.

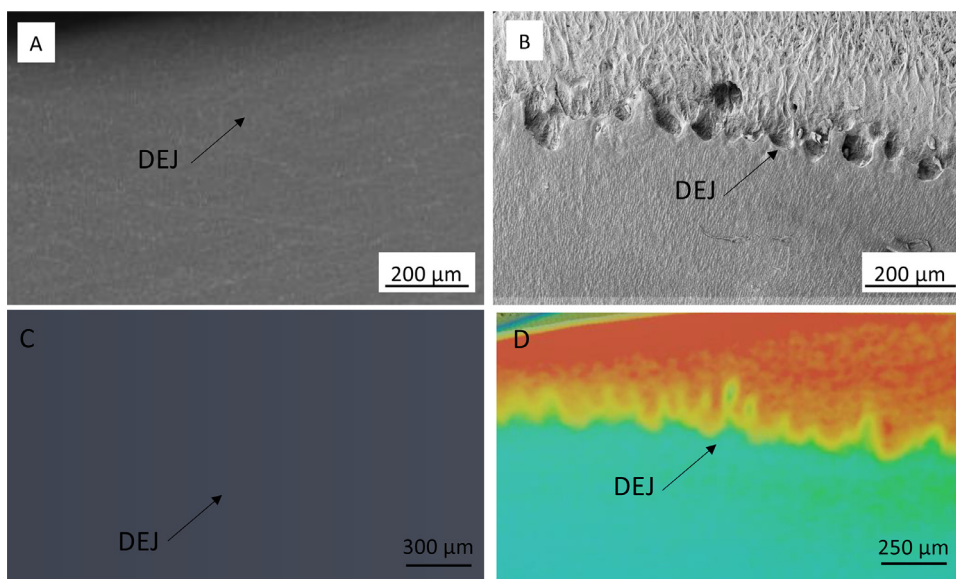


Fig. 7. SEM and micro-CT images of the dentin-enamel junction (DEJ) in the teeth of *Pygocentrus nattereri* (piranha) and *Colossoma Macropomum* (pacu). A) SEM micrograph of a longitudinal cross section of the piranha tooth showing the relatively smooth DEJ. B) SEM micrograph of a longitudinal cross section of the pacu tooth showing the sutured DEJ that contains a combination of triangular and trapezoidal shaped interfaces. C) Micro-CT image of the piranha tooth in pseudo-color showing again the relatively flat interface of the DEJ. D) Micro-CT image of the pacu tooth in pseudo-color showing the interlocking interface of the DEJ.

hibit a highly mineralized reinforcing layer which surrounds the tubule as denoted by the brighter regions in the SEM in Fig. 6.

3.4.3. Dentin-enamel junction

The dentin-enamel junction (DEJ) of the pacu teeth has a distinct interlocking interface while on a similar length-scale the piranha DEJ is relatively smooth and uninterrupted (Fig. 7). This interdigitating suture interface is found across a variety of biological materials (carapace of the red-eared slider [58], mammalian skulls [59], boxfish scute junctions [60], and diatom frustules [61]) and is known to provide intrinsic strength and flexibility to material interfaces [62]. The DEJ plays a critical role in maintaining the biomechanical integrity of the teeth by joining the hard, brittle enamel and subjacent softer, tougher dentin. Thus, it provides a crack arresting barrier. Its resistance to mechanical failure and delamination is predominantly attributed to the presence of collagen fibrils which bridge the DEJ, acting as a fiber-reinforced composite. The DEJ of mammalian teeth has been characterized as having a similar scalloped interface although it is much less angular than the DEJ of the pacu [63–65]. This scalloped interface has been shown to effectively support the mechanical performance during mastication by reducing stress concentrations at the interface and preventing sliding of the underlying dentin layer [66]. A study on the scallop interface in permanent human teeth by Brauer et al. [67] found a relationship between tooth position and scallop size,

where the most posterior teeth (higher masticatory loads) were shown to have larger and more pronounced scallops. This suggests that a scalloped interface benefits teeth which undergo significant stresses due to crushing and grinding.

The suture structure seen in the pacu teeth ranges from triangular to trapezoidal and is much less rounded and more irregular than the scalloped interface seen in mammals [67]. Despite differences in geometry, we suggest that the DEJ found in the pacu serves a similar function as that reported by the scalloped interface in mammals. Suture geometry is important in determining stiffness, strength, failure modes, and stress distribution and can be tailored to optimize mechanical performance [68]. We suggest that the interlocking nature of the DEJ in the pacu teeth helps to enhance mechanical bonding between the dentin and enamel and effectively distributes the stress field during compression making it advantageous for a durophagous diet.

3.5. Compositional analysis by energy dispersive spectroscopy

Quantitative elemental analysis of the piranha and pacu teeth was performed using energy dispersive spectroscopy (EDS). False-colored maps of calcium (blue), phosphorus (pink), and iron (teal) in longitudinal and transversally polished sections of the pacu and piranha teeth is shown in Fig. 8. Both pacu and piranha are observed to have large concentrations of calcium and phospho-

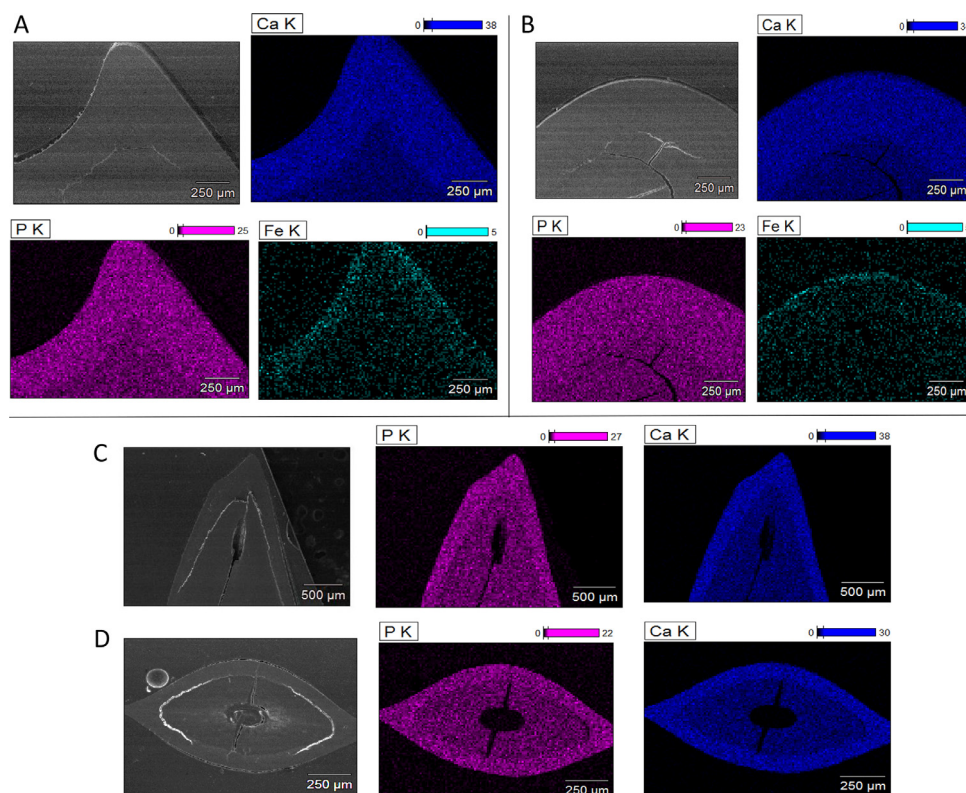


Fig. 8. Energy dispersive X-ray spectroscopy maps of the *Pygocentrus nattereri* (piranha) and *Colossoma Macropomum* (pacu) teeth showing the relative dispersion of Ca, P, and Fe in false-color. A) Longitudinal cross-section of the pacu tooth showing false-colored maps of calcium (blue), phosphorus (pink), and iron (teal). Iron is localized in the cuticle and decreases in a gradient fashion towards the center. There are concentrations of iron on the concave and buccal surfaces. B) Transverse cross section of the pacu tooth showing the relative dispersion of Ca, P, and Fe. While iron is still present in the cuticle and shows to be distributed across a gradient, the transverse section is inherently further away from the tip which may be why the concentration is respectively lower than the transverse surface. C) Longitudinal cross section of the piranha tooth. D) Transverse cross section of the piranha tooth.

Table 1

Concentration of iron in various layers of the piranha and pacu teeth. There is a gradient which is highest in the outermost layer (cuticle) and decreases inwards towards the dentin. This data is taken from point-scans of EDS.

Species	Iron concentration (at.%)				
	Inner dentin	Outer dentin	Inner enameloid	Outer enameloid	Cuticle
<i>Colossoma Macropomum</i> (Pacu)	0	0.17 ± 0.02	0.19 ± 0.03	0.80 ± 0.04	1.69 ± 0.08
<i>Pygocentrus nattereri</i> (Piranha)	0	0	0	0.03 ± 0.02	0.40 ± 0.03

rous which is indicative of hydroxyapatite $\text{Ca}_{10}(\text{PO}_4)_6(\text{OH})_2$. Calcium and phosphorous occur in greater quantities in the enameloid as indicated by the brighter regions in both the piranha and pacu. This is in agreement with the enameloid layer being more mineralized than the underlying dentin layer.

Additionally, iron is present in both teeth but in different quantities. Iron occurs in significantly greater amounts in the pacu teeth than the piranha teeth. Iron in the pacu teeth occurs in such large quantities that it is referred to as pigmented enameloid, forming an observable rust-colored layer (Fig. 8A and S2). In the piranha, the presence of iron is considerably less and cannot be visualized in the EDS maps but can be detected by point analysis. In both teeth, iron is greatest in the cuticle for the pacu (1.69 ± 0.08 at%) and piranha (0.40 ± 0.03 at%) and gradually diminishes towards the center of the tooth towards the dentin (Table 1). For the pacu, there are trace amounts of iron that reach the outer-dentin layer, while in the piranha detectable iron only reaches as far as the outer-enameloid layer. The iron is not uniformly distributed in the pacu cuticle layer as larger concentrations are found on the concave and lingual surfaces with minimal iron at the occlusal surface (tip). This may be due to an increase in wear at the tip during

the lifetime of the tooth as a result of its durophagous diet. Ferric iron has been reported in butterflyfish teeth (Chaetodontidae, Perciformes) and found in higher concentrations for species who specialize in feeding on hard-bodied prey [69].

3.6. Nanoindentation of enameloid and dentin layers

Modulus and hardness maps of the longitudinal and transverse cross sections of the teeth reveal that the stiffest and hardest portion occurs in the cuticle layer and is at a minimum in the dentin layer. This is in agreement with the compositional gradients in mineralization and iron which are greatest in the cuticle layer and decrease towards the dentin. The cuticle of the pacu teeth (5.8 ± 0.2 GPa) is found to be harder than that for the piranha teeth (4.9 ± 0.6 GPa) (Fig. 9). This is not surprising as the pacu cuticle has a significantly larger concentration of iron which increases the hardness. The hardness of the cuticle of the pacu teeth is comparable to the pigmented enamel found in beaver teeth (5.9 ± 0.3 GPa) where the high hardness is also due to iron [42]. Despite the high hardness in the pacu cuticle, the piranha cuticle is significantly stiffer, with a modulus of 104 ± 11 GPa compared to the modu-

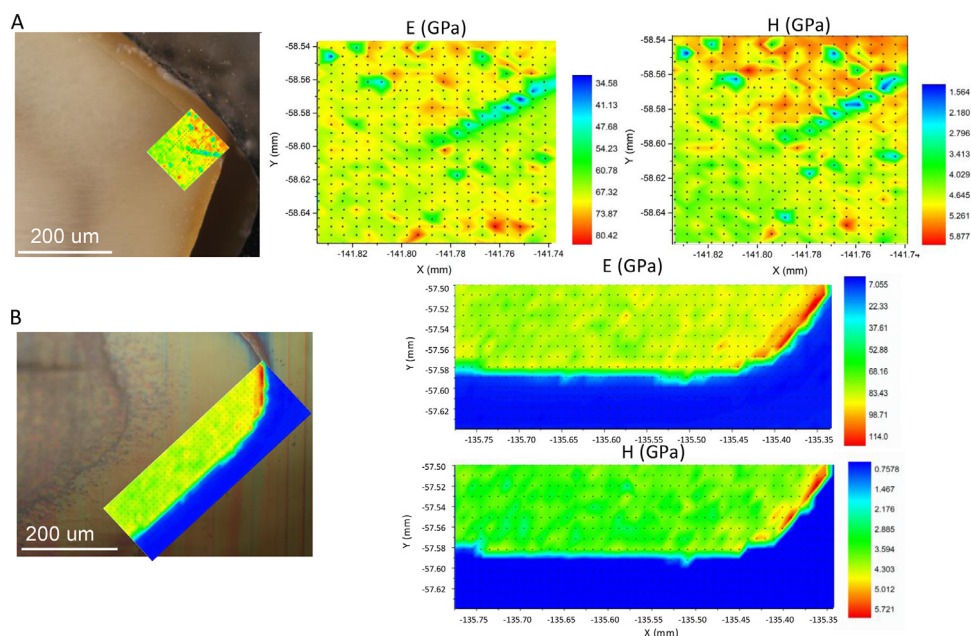


Fig. 9. Nanoindentation characterization of longitudinal sections of cuticle and enameloid layers in the *Pygocentrus nattereri* (piranha) and *Colossoma Macropomum* (pacu) teeth of modulus (E) and hardness (H). A) Pacu tooth, noting the pigmented cuticle in the optical micrograph. B) Piranha tooth.

lus of the pacu cuticle of 79 ± 2 GPa. This can be explained by the piranha teeth typically having a higher degree of mineralization [41]. Additionally, the comparatively lower modulus measured in the pacu teeth can be the result of the lesser degree of mineralization. The local mechanical response of the cuticle layer in the pacu and the piranha is consistent with their specialized diets. Having a stiff cuticle is beneficial for the piranha to maintain its rigidity as it effectively pierces through prey, while a high degree of hardness provides the necessary strength and wear resistance for the crushing and grinding mechanisms necessary for the pacu's durophagous diet.

Despite large differences in the mechanical properties in the cuticle layers, the enameloid and dentin are relatively similar in the pacu and piranha (Fig. 10). The modulus of the enameloid in the teeth in the longitudinal and transverse orientations are 83 ± 5 GPa and 77 ± 5 GPa for the piranha and 73 ± 7 GPa and 76 ± 5 GPa for the pacu. Thus, the enameloid of the piranha is only slightly stiffer than that of the pacu which again can be related to its high degree of mineralization and functional constraints of rigidity. The inner enameloid can be described, by virtue of its three-dimensional interwoven structure, as isotropic while the directionality of the parallel orientated structuring in the outer enameloid lends itself to being more anisotropic. It is likely that differences in these layers within the enameloid were captured in the piranha teeth. Despite the pacu having a higher iron content in the enameloid, it is not significantly harder than the piranha which is likely due to differences in mineralization. The pacu is less mineralized but the presence of iron can supplement this deficiency. When iron substitutes for calcium in hydroxyapatite, the iron-oxygen is less ionic and more polar-covalent bond which is stronger than the calcium-oxygen ionic bond [70]. It is possible that being less mineralized is more favorable for damage tolerance.

Similar to the trend seen in the cuticle layer, the hardness of the enameloid is slightly greater in the pacu teeth than the piranha teeth in both orientations. The hardness of the enameloid in the longitudinal and transverse orientation for the pacu teeth are 3.7 ± 0.6 GPa and 3.8 ± 0.4 GPa while the piranha teeth are 3.7 ± 0.4 GPa and 2.9 ± 0.4 GPa respectively. Again, this hardness can be attributed to the higher degree of iron in the enameloid

layer of the pacu teeth than the piranha teeth. The hardness of the piranha teeth is significantly different in the longitudinal and transverse orientations while in the pacu teeth there is no significant difference. Both the hardness and modulus of the enameloid occur in a gradient with higher values towards the exterior of the tooth as can be seen best in Fig. 10.

The modulus of the dentin layers is the most consistent with respect to orientation and in the piranha is found to be 23 ± 8 GPa for the longitudinal and 23 ± 3 GPa for the transverse cross sections. For the pacu, the moduli of the dentin layer are 22 ± 3 GPa and 22 ± 3 GPa, respectively. Similar to the cuticle and enameloid layers, the modulus of the dentin is larger in the piranha teeth than the pacu teeth but the difference is minor. The hardness of the dentin layer for the piranha in the longitudinal cross section is 1.1 ± 0.5 GPa and in the transverse is 0.72 ± 0.2 . A similar range of hardness is found in the dentin layer of the pacu at 0.9 ± 0.2 GPa for the longitudinal cross section and 1.0 ± 0.3 GPa for the transverse cross section. The modulus and hardness with respect to the longitudinal and transverse orientations across the cuticle, enameloid, and dentin are summarized in Table 2.

3.7. Modeling

In order to better understand how tooth shape and enameloid thickness influences stress distribution within the tooth during compression, we performed computational simulations on the most anterior teeth of the piranha and pacu using the finite element software Abaqus (v.6.14). This methodology has been previously applied to better understand the biomechanics of shark teeth upon penetration [71]. A three-dimensional representation of each tooth was obtained using X-ray micro-computed tomography and subsequently digitized into an appropriate mesh to obtain the CAD geometry. It is important to use a non-homogenous model to account for both the dentin and enameloid material properties as it has been shown that a major portion of the load is primarily supported by the enamel layer in mammalian teeth [72]. Each model was divided into two mechanically distinct regions which were modeled with a linear elastic model with Young's modulus obtained directly from the nanoindentation experiments: piranha

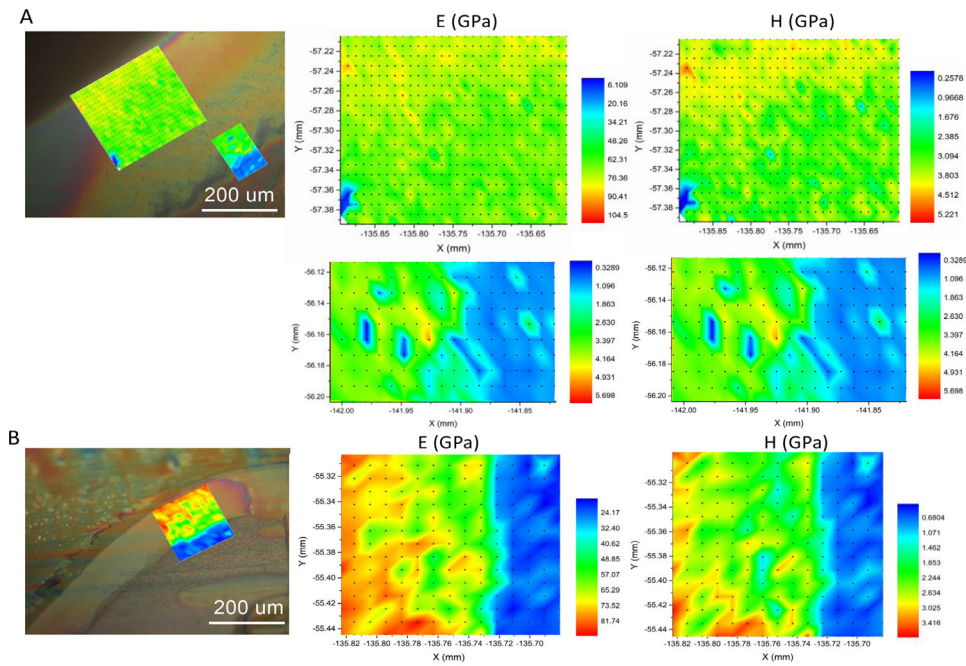


Fig. 10. Nanoindentation characterization of transverse cross sections of enameloid and dentin layers in the *Pygocentrus nattereri* (piranha) and *Collossoma Macropomum* (pacu) teeth representing modulus (E) and hardness (H). A) Pacu tooth, notice the gradient in modulus and hardness from the OE to the IE (yellow to green) B) Piranha tooth with a similar gradient.

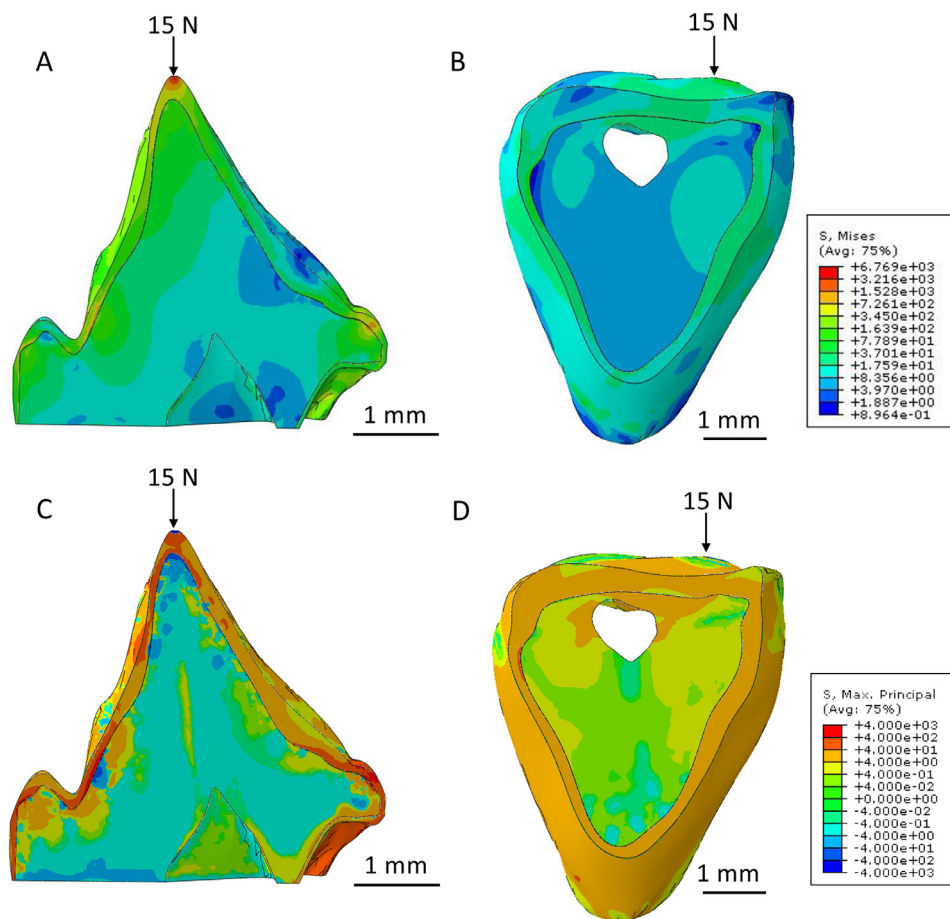


Fig. 11. Finite element analysis of longitudinal cross sections of anterior *Pygocentrus nattereri* (piranha) and *Collossoma Macropomum* (pacu) dentition under compression with a load of 15 N. Distribution of stresses is dependent on the size of the tooth, morphology, and enameloid thickness. A) The piranha tooth exhibits high stress concentration at the tip in regards to von Mises stress. B) The pacu tooth more evenly distributes the applied stress which is minimized at the thicker cusps of the enameloid with regards to von Mises stress. C) Maximum principal stress of the piranha tooth shows high tensile stresses occurring in the enameloid and compressive stresses occurring in the dentin. D) Maximum principal stress of the pacu tooth is greatly reduced. Units: MPa.

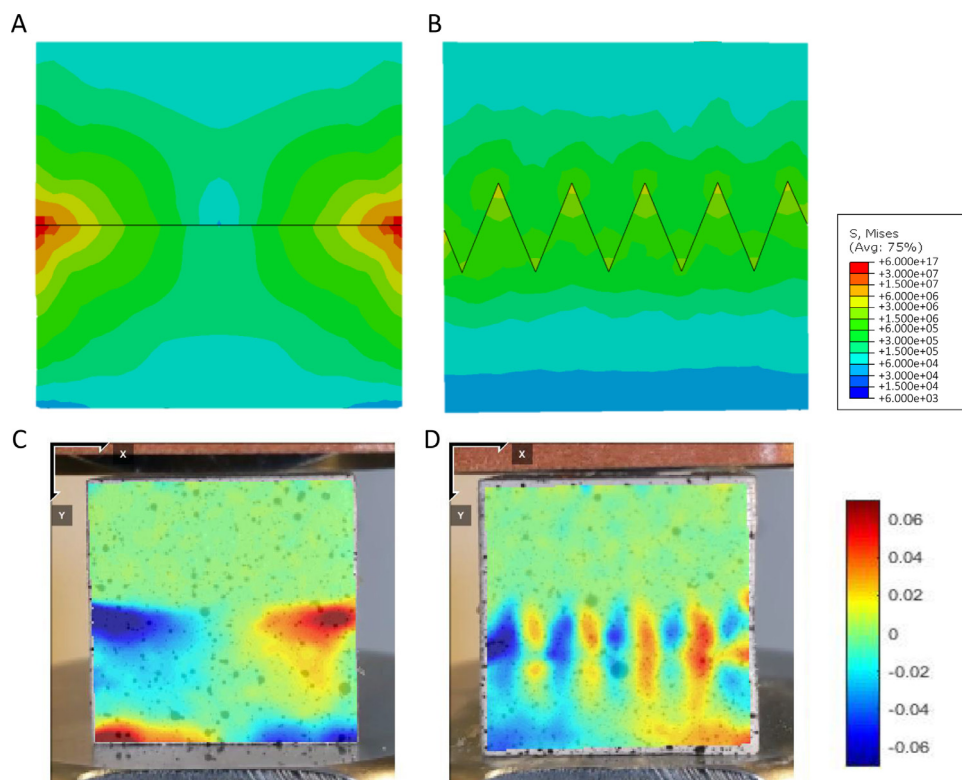


Fig. 12. Interfaces inspired by *Pygocentrus nattereri* (piranha) and *Colossoma Macropomum* (pacu). A) FEA results of the flat interface inspired by the DEJ of the piranha showing stress concentrations at the edges. B) FEA results of the interlocking triangular interface inspired by the DEJ of the pacu showing how the stress is more evenly distributed. Units: MPa C) DIC analysis of the shear strain in the flat 3D printed interface. D) DIC analysis of the shear strain in the 3D printed sutured interface.

Table 2
Modulus and hardness from nanoindentation of *Pygocentrus nattereri* (piranha) and *Colossoma Macropomum* (pacu) across the cuticle, enameloid, and dentin with respect to the longitudinal and transverse direction (mean ± standard deviation).

	<i>Pygocentrus nattereri</i> (Piranha)		<i>Colossoma Macropomum</i> (Pacu)	
	Longitudinal	Transverse	Longitudinal	Transverse
Cuticle modulus (GPa)	104 ± 11	–	79 ± 2	–
Cuticle hardness (GPa)	4.9 ± 0.6	–	5.8 ± 0.2	–
Enameloid modulus (GPa)	83 ± 5	77 ± 6	73 ± 7.0	76 ± 5
Enameloid hardness (GPa)	3.7 ± 0.4	2.9 ± 0.4	3.7 ± 0.6	3.8 ± 0.4
Dentin modulus (GPa)	23 ± 8	23 ± 3	22 ± 3	22 ± 4
Dentin hardness (GPa)	1.1 ± 0.5	0.7 ± 0.2	0.9 ± 0.2	1.0 ± 0.3

enameloid ($E = 80$ GPa), piranha dentin ($E = 23$ GPa), pacu enameloid (75 GPa), and pacu dentin (22 GPa). A force of 15 N was translated to a pressure dependent on the area of the tip of each tooth. This force was used as it was attainable by both species when compared to the theoretical anterior bite forces and was sufficiently high for both replicative diets (enough force to initiate a crack in a hard-shelled fruit and to penetrate flesh). The piranha tooth was fixed at the base of the tooth, while the pacu tooth was fixed on the exposed edges of its lingual surfaces. This is representative of the attachment of the teeth to the jaw.

The stress distribution in each tooth under compression is revealed by the finite element model. In Fig. 11A and B, von Mises stresses are mainly distributed within the enameloid and reduced in the dentin layer. The piranha localizes stresses at the tip, while the broad cusps of the pacu teeth help to more evenly distribute the stress. The curvature of the piranha tooth leads to an uneven stress distribution within the enameloid with higher stresses occurring on the concave side. The portion of the piranha tooth that would interlock with its neighboring tooth shows a localized concentration of stress in the enameloid. While only one tooth

was simulated, the interlocking nature of the piranha teeth may help to distribute this stress. When looking at the principal maximum stress the enameloid is under tension while the dentin is under compression. From this, we can predict failure to occur in the enameloid with higher concentrations occurring near the DEJ due to the enameloid bending over the softer underlying dentin layer, leaving the dentin layer in compression. Additionally, the piranha tooth sees higher tensile stresses near the tip due to the small dentin horn angle. Correspondence of dentin horn angle and enameloid thickness are known to influence fracture resistance [73].

The thicker enameloid in the pacu leads to a reduction in the stress within the enameloid and dentin layers (Fig. 11B and D). The tensile stresses in the enameloid are significantly reduced when compared to the piranha. This is due to the lack of a dentin horn angle and a relatively broad cusp. Additionally, the thickest parts of the enameloid in the pacu show a reduction in stress. The more evenly distributed and minimized von Mises and maximum principal stress may also be attributed to the differing boundary conditions and how each tooth is attached to the jaw. The stress dis-

tribution pattern in the pacu teeth suggests greater efficiency and lower deformation during compression when compared to the piranha teeth.

3.8. Bioinspired suture interfaces

This study demonstrates that the pacu teeth are hierarchically structured to better respond to compressive forces than the piranha teeth. One important microstructural feature that contributes to this is the sutured interface of the DEJ. Here we use a simplified prototype inspired by the suturing in the DEJ of both the piranha and the pacu to better understand the mechanisms at hand. Two prototypes (flat interface vs sutured) are analyzed using numerical modeling and 3D printed and mechanically tested using quasi-static compression paired with digital image correlation to visualize the strains. Both prototypes are composed of two layers: a stiff layer (Veroclear, $E = 2.3$ GPa) meant to represent the enameloid which is stacked upon a softer layer (Flex9985, $E = 1.1$ GPa) meant to represent dentin. The sutured interface is triangular with a 45° tip angle.

Using FEA we compare two layered structures with different interfaces: (1) flat inspired by the piranha and (2) triangular sutures inspired by the pacu. In Fig. 12, the stress is more evenly distributed under compression when there is an interlocking interface. Most importantly, the maximum stresses are concentrated on the tips of the triangles that terminate into the inner enameloid and are thus disconnected. This localizes and constrains the maximum stress in the enameloid. The microstructure of the inner enameloid, being interwoven, likely inhibits crack growth that may initiate at these sites. With a flat interface the stress concentrates on both sides of the interface—there are large stresses both in the enameloid and dentin regions. This simple design provides insight into how the structuring of the DEJ works cooperatively with the microstructure of the inner enameloid and enables the pacu to fulfill a durophagous diet.

Using digital image correlation, we compared the two layered structures (Fig. 12C and D) to determine how the triangular interlocking interface influences the strain distribution. With a flat interface the shear strain concentrates on the corners of the interface and at the base of the structure. With a sutured interface the shear strain decreases and is more uniformly distributed.

4. Conclusions

The teeth of the piranha and the pacu are complex hierarchical composites optimized for their respective diets: primarily soft flesh for the piranha and durophagous for the pacu. These require notable differences in tooth morphology, microstructure, composition, and mechanical properties. The main findings of this research are:

- The bite force of the piranha is higher than that of the pacu, for the same standard length of fish, confirming recent results by Huby et al. [41].
- The enameloid thickness is higher and more irregular for the pacu.
- The dentin-enameloid-junction in the pacu exhibits a suture morphology, whereas it is absent in the piranha. We demonstrate, using FEA and a model produced by additive manufacturing, that the suture morphology at the dentin-enameloid interface decreases the interfacial stresses.
- The hardness of the cuticle layer in the pacu teeth is due to the greater concentrations of iron present, while the tip of the piranha teeth demonstrates greater stiffness.
- The pacu teeth are more suited for withstanding large compressive loads when compared to their carnivorous counterpart whose dentition is optimized for slicing.

- These factors may provide insights into the design and fabrication of layered materials with suture interfaces for applications that require compressive loading conditions.

Data and materials availability

All data needed to evaluate the conclusions in the paper are present in the paper and/or the Supplementary Materials. Additional data related to this paper may be requested from the authors

Declaration of Competing Interest

The authors declare no competing financial interests.

We wish to confirm that there are no known conflicts of interest associated with this publication and there has been no significant financial support for this work that could have influenced its outcome.

All of the sources of funding for the work described in this publication are acknowledged below:

This work was supported by the Multidisciplinary University Research Initiative to University of California Riverside, funded by the Air Force Office of Scientific Research (AFOSR-FA9550-15-1-0009), with subcontracts to UC San Diego. This funding was used for experiments, characterization, and writing of the manuscript. This work was performed in part at the San Diego Nanotechnology Infrastructure (SDNI) of UCSD, a member of the National Nanotechnology Coordinated Infrastructure (NNCI), which is supported by the National Science Foundation (Grant ECCS-1542148).

CRediT authorship contribution statement

Audrey Velasco-Hogan: Conceptualization, Methodology, Formal analysis, Investigation, Writing – original draft, Writing – review & editing, Visualization, Funding acquisition. **Wei Huang:** Methodology, Formal analysis, Investigation, Writing – review & editing. **Carlos Serrano:** Investigation. **David Kisailus:** Resources, Supervision. **Marc A. Meyers:** Conceptualization, Resources, Writing – review & editing, Visualization, Supervision, Funding acquisition.

Acknowledgements

This work was performed in part at the San Diego Nanotechnology Infrastructure (SDNI) of UCSD, a member of the National Nanotechnology Coordinated Infrastructure (NNCI), which is supported by the National Science Foundation (Grant ECCS-1542148). M.A.M. thanks Air Force Office of Scientific Research for support under the MURI Program (AFOSR Grant No. FA9550-15-0009). A.V.H. and C.S. thank UCSD for support under the Chancellor's Interdisciplinary Collaboratories funding. We thank Eric Bushong for his expertise with x-ray microscopy. The measurements on piranha were accomplished during the Roosevelt-Rondon Centennial Expedition, from 2014 to 2016. The participation of the New York Explorers Club by giving it an official Flag Expedition status, is warmly appreciated, as are the efforts of Colonels Hiram Reis de Silva and Ivan Carlos Angonese of the Brazilian Army. Drs. Julie and Tim Radke of the San Diego Explorers Club participated in the Paraguay River journey and their contribution was essential. The Brazilian Army provided logistic support which enabled the expedition. We thank Isaac Cabrera for helpful discussions and insight on computational modeling. We thank Steve Naleway for his initial interest in the investigation of the jaws of the piranha and pacu and for his guidance in discussions. We thank Joanna McKittrick for all of her contributions and inspiration to the field of structural biological materials.

Supplementary materials

Supplementary material associated with this article can be found, in the online version, at doi:[10.1016/j.actbio.2021.08.024](https://doi.org/10.1016/j.actbio.2021.08.024).

References

- P.S. Ungar, Mammal teeth: origin, evolution, and diversity, 2010. doi:[10.5860/choice.48-3875](https://doi.org/10.5860/choice.48-3875).
- L.P. Bergqvist, The role of teeth in mammal history, *Braz. J. Oral Sci.* (2003).
- P. Lucas, P. Constantino, B. Wood, B. Lawn, Dental enamel as a dietary indicator in mammals, *Bioessays* (2008), doi:[10.1002/bies.20729](https://doi.org/10.1002/bies.20729).
- P.S. Ungar, Mammalian dental function and wear: a review, *Biosurf. Biotribol.* (2015), doi:[10.1016/j.bsbt.2014.12.001](https://doi.org/10.1016/j.bsbt.2014.12.001).
- A.H. Jheon, K. Seidel, B. Biehls, O.D. Klein, From molecules to mastication: the development and evolution of teeth, *Wiley Interdiscip. Rev. Dev. Biol.* (2013), doi:[10.1002/wdev.63](https://doi.org/10.1002/wdev.63).
- W. Maier, Tooth Morphology and Dietary Specialization, *Food Acquis. Process. Primates*, 1984, doi:[10.1007/978-1-4757-5244-1_13](https://doi.org/10.1007/978-1-4757-5244-1_13).
- D.S. Koussoulakou, L.H. Margaritis, S.L. Koussoulakos, A curriculum vitae of teeth: evolution, generation, regeneration, *Int. J. Biol. Sci.* (2009), doi:[10.7150/ijbs.5.226](https://doi.org/10.7150/ijbs.5.226).
- P.W. Lucas, Dental Functional Morphology, 2004, doi:[10.1017/cbo9780511735011](https://doi.org/10.1017/cbo9780511735011).
- P.C.J. Donoghue, M. Rücklin, The ins and outs of the evolutionary origin of teeth, *Evol. Dev.* (2016), doi:[10.1111/ede.12099](https://doi.org/10.1111/ede.12099).
- B. Berkovitz, P. Shellis, The Teeth of Non-Mammalian Vertebrates, 2016. doi:[10.1016/c2014-0-02210-1](https://doi.org/10.1016/c2014-0-02210-1).
- B. Berkovitz, P. Shellis, Tooth formation, Teeth Non-Mammalian Vertebr., 2017, doi:[10.1016/b978-0-12-802850-6.00009-6](https://doi.org/10.1016/b978-0-12-802850-6.00009-6).
- B. Berkovitz, P. Shellis, Enameloid and enamel, Teeth Non-Mammalian Vertebr., 2017, doi:[10.1016/b978-0-12-802850-6.00012-6](https://doi.org/10.1016/b978-0-12-802850-6.00012-6).
- I. Sasagawa, M. Ishiyama, H. Yokosuka, M. Mikami, T. Uchida, Tooth enamel and enameloid in actinopterygian fish, *Front. Mater. Sci. China*, 2009, doi:[10.1007/s11706-009-0030-3](https://doi.org/10.1007/s11706-009-0030-3).
- B. Berkovitz, P. Shellis, Dentine and dental pulp, Teeth Non-Mammalian Vertebr., 2017, doi:[10.1016/b978-0-12-802850-6.00011-4](https://doi.org/10.1016/b978-0-12-802850-6.00011-4).
- P.C. Wainwright, D.R. Bellwood, Ecomorphology of feeding in coral reef fishes, *Coral Reef Fishes*, 2002, doi:[10.1016/b978-012615185-5/50004-9](https://doi.org/10.1016/b978-012615185-5/50004-9).
- K.F. Liem, Acquisition of energy by teleosts: adaptive mechanisms and evolutionary patterns, *Environ. Physiol. Fishes* (1980), doi:[10.1007/978-1-4899-3659-2_10](https://doi.org/10.1007/978-1-4899-3659-2_10).
- P.C. Wainwright, S.H. Huskey, R.G. Turingan, A.M. Carroll, Ontogeny of suction feeding capacity in snook, *Centropomus undecimalis*, *J. Exp. Zool. Part A* (2006), doi:[10.1002/jez.a.255](https://doi.org/10.1002/jez.a.255).
- P. Wainwright, A.M. Carroll, D.C. Collar, S.W. Day, T.E. Higham, R.A. Holzman, Suction feeding mechanics, performance, and diversity in fishes, *Integr. Comp. Biol.* (2007), doi:[10.1093/icb/pcm032](https://doi.org/10.1093/icb/pcm032).
- P.C. Wainwright, B.A. Richard, Predicting patterns of prey use from morphology of fishes, *Environ. Biol. Fishes* (1995), doi:[10.1007/BF00005909](https://doi.org/10.1007/BF00005909).
- M.J. Sonnefeld, R.G. Turingan, T.J. Sloan, Functional morphological drivers of feeding mode in marine teleost fishes, *Adv. Zool. Bot.* (2014).
- A.W. Thompson, R. Betancur-R, H. López-Fernández, G. Orti, A time-calibrated, multi-locus phylogeny of piranhas and pacus (Characiformes: serrasalmidae) and a comparison of species tree methods, *Mol. Phylogenet. Evol.* (2014), doi:[10.1016/j.ympev.2014.06.018](https://doi.org/10.1016/j.ympev.2014.06.018).
- M.A. Kolmann, K.E. Cohen, K.E. Bemis, A.P. Summers, F.J. Irish, L.P. Hernandez, Tooth and consequences: heterodonty and dental replacement in piranhas and pacus (Serrasalmidae), *Evol. Dev.* 21 (2019) 278–293, doi:[10.1111/ede.12306](https://doi.org/10.1111/ede.12306).
- J.R. Grubich, S. Huskey, S. Crofts, G. Orti, J. Porto, Mega-Bites: extreme jaw forces of living and extinct piranhas (Serrasalmidae), *Sci. Rep.* 2 (2012), doi:[10.1038/srep01009](https://doi.org/10.1038/srep01009).
- T.G. Northcote, R.G. Northcote, M.S. Arcifa, Differential cropping of the caudal fin lobes of prey fishes by the piranha, *Serrasalmus spilopleura* Kner, *Hydrobiologia* (1986), doi:[10.1007/BF00014215](https://doi.org/10.1007/BF00014215).
- A.T. da Silva, J. Zina, F.C. Ferreira, L.M. Gomiero, R. Goitein, Caudal fin-nipping by serrasalmus maculatus (Characiformes: serrasalmidae) in a small water reservoir: seasonal variation and prey selection, *Zoologia* (2015), doi:[10.1590/S1984-46702015000600004](https://doi.org/10.1590/S1984-46702015000600004).
- R.P. Shellis, B.K.B. Berkovitz, Observations on the dental anatomy of piranhas (Characidae) with special reference to tooth structure, *J. Zool.* (1976), doi:[10.1111/j.1469-7998.1976.tb04664.x](https://doi.org/10.1111/j.1469-7998.1976.tb04664.x).
- W.E. Burgess, Check List of the Freshwater Fishes of South and Central America, *Copeia* (2004), doi:[10.1643/ot-04-142](https://doi.org/10.1643/ot-04-142).
- M.C. Andrade, T. Giarrizzo, M. Jégu, Tometes camunani (Characiformes: Serrasalmidae), a new species of phytophagous fish from the Guiana Shield, rio Trombetas basin, Brazil, *Neotrop. Ichthyol.* (2013), doi:[10.1590/S1679-62252013000200008](https://doi.org/10.1590/S1679-62252013000200008).
- S.B. Correa, K.O. Winemiller, H. López-Fernández, M. Galetti, Evolutionary perspectives on seed consumption and dispersal by fishes, *Bioscience* (2007), doi:[10.1641/b570907](https://doi.org/10.1641/b570907).
- G.T. Prance, M. Goulding, The fishes and the forest: explorations in amazonian natural history, *Brittonia* 33 (1981) 257, doi:[10.2307/2806336](https://doi.org/10.2307/2806336).
- M. Goulding, M.L. Carvalho, Life history and management of the tambaqui (*Colossoma macropomum*, Characidae): an important Amazonian food fish, *Rev. Bras. Zool.* (1982), doi:[10.1590/s0101-81751982000200001](https://doi.org/10.1590/s0101-81751982000200001).
- W.-E. Reif, Morphogenesis, pattern formation and function of the dentition of Heterodontus (Selachii), *Zoomorphologie* 83 (1976) 1–47, doi:[10.1007/BF00995429](https://doi.org/10.1007/BF00995429).
- M.A. Kolmann, R. Dean Grubbs, D.R. Huber, R. Fisher, N.R. Lovejoy, G.M. Erickson, Intraspecific variation in feeding mechanics and bite force in durophagous stingrays, *J. Zool.* (2018), doi:[10.1111/jzo.12530](https://doi.org/10.1111/jzo.12530).
- D.R. Huber, T.G. Eason, R.E. Hueter, P.J. Motta, Analysis of the bite force and mechanical design of the feeding mechanism of the durophagous horn shark *Heterodontus francisci*, *J. Exp. Biol.* (2005), doi:[10.1242/jeb.01816](https://doi.org/10.1242/jeb.01816).
- R.S. Mehta, Ecomorphology of the moray bite: relationship between dietary extremes and morphological diversity, *Physiol. Biochem. Zool.* (2009), doi:[10.1086/594381](https://doi.org/10.1086/594381).
- A. Herrel, S. Petrochic, M. Draud, Sexual dimorphism, bite force and diet in the diamondback terrapin, *J. Zool.* (2018), doi:[10.1111/jzo.12520](https://doi.org/10.1111/jzo.12520).
- A. Herrel, V. Holanova, Cranial morphology and bite force in Chamaeleolis lizards - Adaptations to molluscivory? *Zoology* (2008), doi:[10.1016/j.zool.2008.01.002](https://doi.org/10.1016/j.zool.2008.01.002).
- A. Herrel, J.C. O'Reilly, A.M. Richmond, Evolution of bite performance in turtles, *J. Evol. Biol.* (2002), doi:[10.1046/j.1420-9101.2002.00459.x](https://doi.org/10.1046/j.1420-9101.2002.00459.x).
- A. Huby, A. Lowie, A. Herrel, R. Vigouroux, F. Bruno, X. Raick, G. Kurchevski, A.L. Godinho, E. Parmentier, Functional diversity in biters: the evolutionary morphology of the oral jaw system in pacus, piranhas and relatives (Teleostei: serrasalmidae), *Biol. J. Linn. Soc.* 127 (2019) 722–741, doi:[10.1093/biolinnean/blz048/5486927](https://doi.org/10.1093/biolinnean/blz048/5486927).
- K.R. Mara, P.J. Motta, D.R. Huber, Bite force and performance in the durophagous bonnethead shark, *Sphyrna tiburo*, *J. Exp. Zool. Part A* (2010), doi:[10.1002/jez.576](https://doi.org/10.1002/jez.576).
- Y. Delaunois, A. Huby, C. Malherbe, G. Eppe, É. Parmentier, P. Compère, Microstructural and compositional variation in pacu and piranha teeth related to diet specialization (Teleostei: Serrasalmidae), *J. Struct. Biol.* (2020), doi:[10.1016/j.jsb.2020.107509](https://doi.org/10.1016/j.jsb.2020.107509).
- L.M. Gordon, M.J. Cohen, K.W. MacRenaris, J.D. Pasteris, T. Seda, D. Joester, Amorphous intergranular phases control the properties of rodent tooth enamel, *Science* 347 (2015) 746–750, doi:[10.1126/science.1258950](https://doi.org/10.1126/science.1258950).
- P.-Y. Chen, J. Schirer, A. Simpson, R. Nay, Y.S. Lin, W. Yang, M.I. Lopez, J. Li, E.A. Olevsky, M.A. Meyers, Predation versus protection: fish teeth and scales evaluated by nanoindentation, *J. Mater. Res.* 27 (2012) 100–112, doi:[10.1557/jmr.2011.332](https://doi.org/10.1557/jmr.2011.332).
- Y.F. Jia, F.Z. Xuan, Anisotropic fatigue behavior of human enamel characterized by multi-cycling nanoindentation, *J. Mech. Behav. Biomed. Mater.* (2012), doi:[10.1016/j.jmbbm.2012.10.008](https://doi.org/10.1016/j.jmbbm.2012.10.008).
- Y.R. Jeng, T.T. Lin, H.M. Hsu, H.J. Chang, D. Bin Shieh, Human enamel rod presents anisotropic nanotribological properties, *J. Mech. Behav. Biomed. Mater.* (2011), doi:[10.1016/j.jmbbm.2010.12.002](https://doi.org/10.1016/j.jmbbm.2010.12.002).
- M. Yahyazadehfar, D. Bajaj, D.D. Arola, Hidden contributions of the enamel rods on the fracture resistance of human teeth, *Acta Biomater* (2013), doi:[10.1016/j.actbio.2012.09.020](https://doi.org/10.1016/j.actbio.2012.09.020).
- H.H.K. Xu, D.T. Smith, S. Jahanmir, E. Romberg, J.R. Kelly, V.P. Thompson, E.D. Rekow, Indentation damage and mechanical properties of human enamel and dentin, *J. Dent. Res.* (1998), doi:[10.1177/00220345980770030601](https://doi.org/10.1177/00220345980770030601).
- M.W. Westnate, A biomechanical model for analysis of muscle force, power output and lower jaw motion in fishes, *J. Theor. Biol.* 223 (2003) 269–281, doi:[10.1016/S0022-5193\(03\)00058-4](https://doi.org/10.1016/S0022-5193(03)00058-4).
- M.A. Meyers, Y.S. Lin, E.A. Olevsky, P.Y. Chen, Battle in the Amazon: arapaima versus piranha, *Adv. Eng. Mater.* 14 (2012) B279–B288, doi:[10.1002/adem.201180027](https://doi.org/10.1002/adem.201180027).
- A. Velasco-Hogan, M.A. Meyers, Bite force mechanics and allometry of piranha (Serrasalmidae), *J. Mech. Behav. Biomed. Mater.* 115 (2021) 104296, doi:[10.1016/j.jmbbm.2020.104296](https://doi.org/10.1016/j.jmbbm.2020.104296).
- L.P. Hernandez, P.J. Motta, Trophic consequences of differential performance: ontogeny of oral jaw-crushing performance in the sheepshead, *Archosargus probatocephalus* (Teleostei, Sparidae), *J. Zool.* (1997) 243, doi:[10.1111/j.1469-7998.1997.tb01973.x](https://doi.org/10.1111/j.1469-7998.1997.tb01973.x).
- L.B. Whitenack, P.J. Motta, Performance of shark teeth during puncture and draw: implications for the mechanics of cutting, *Biol. J. Linn. Soc.* (2010) 100, doi:[10.1111/j.1095-8312.2010.01421.x](https://doi.org/10.1111/j.1095-8312.2010.01421.x).
- J.E. Lambert, C.A. Chapman, R.W. Wrangham, N.Lou Conklin-Brittain, Hardness of cercopithecine foods: implications for the critical function of enamel thickness in exploiting fallback foods, *Am. J. Phys. Anthropol.* (2004), doi:[10.1002/ajpa.10403](https://doi.org/10.1002/ajpa.10403).
- M. Yahyazadehfar, D. Arola, The role of organic proteins on the crack growth resistance of human enamel, *Acta Biomater.* 19 (2015), doi:[10.1016/j.actbio.2015.03.011](https://doi.org/10.1016/j.actbio.2015.03.011).
- O. Borrero-Lopez, P.J. Constantino, M.B. Bush, B.R. Lawn, On the vital role of enamel prism interfaces and graded properties in human tooth survival: human tooth microstructure, *Biol. Lett.* (2020) 16, doi:[10.1098/rsbl.2020.0498](https://doi.org/10.1098/rsbl.2020.0498).
- B. Berkovitz, P. Shellis, in: Chapter 4 - Bony Fishes, Academic Press, 2017, pp. 43–111, doi:[10.1016/B978-0-12-802850-6.00004-7](https://doi.org/10.1016/B978-0-12-802850-6.00004-7). in: B. Berkovitz, P.B.T.-T.T. of N.-M.V. Shellis (Eds.).
- S. Suga, Y. Taki, Fluoride and iron concentrations in the teeth of primitive bony fishes (Osteichthyes), *Hard Tissue Miner. Deminer.* (1992), doi:[10.1007/978-4-431-68183-0_2](https://doi.org/10.1007/978-4-431-68183-0_2).

- [58] S. Krauss, E. Monsonego-Ornan, E. Zelzer, P. Fratzi, R. Shahar, Mechanical function of a complex three-dimensional suture joining the bony elements in the shell of the red-eared slider turtle, *Adv. Mater.* (2009), doi:[10.1002/adma.200801256](https://doi.org/10.1002/adma.200801256).
- [59] C.R. Jaslow, Mechanical properties of cranial sutures, *J. Biomech.* (1990), doi:[10.1016/0021-9290\(90\)90059-C](https://doi.org/10.1016/0021-9290(90)90059-C).
- [60] W. Yang, S.E. Naleway, M.M. Porter, M.A. Meyers, J. McKittrick, The armored carapace of the boxfish, *Acta Biomater.* 23 (2015) 1–10, doi:[10.1016/j.actbio.2015.05.024](https://doi.org/10.1016/j.actbio.2015.05.024).
- [61] I.C. Gebeshuber, J.H. Kindt, J.B. Thompson, Y. Del Amo, H. Stachelberger, M.A. Brzezinski, G.D. Stucky, D.E. Morse, P.K. Hansma, Atomic force microscopy study of living diatoms in ambient conditions, *J. Microsc.* 212 (2003) 292–299, doi:[10.1111/j.1365-2818.2003.01275.x](https://doi.org/10.1111/j.1365-2818.2003.01275.x).
- [62] S.E. Naleway, M.M. Porter, J. McKittrick, M.A. Meyers, Structural Design Elements in Biological Materials: application to Bioinspiration, *Adv. Mater.* 27 (2015) 5455–5476, doi:[10.1002/adma.201502403](https://doi.org/10.1002/adma.201502403).
- [63] A. Nanci, *Ten Cate's Oral Histology*, Elsevier, 2013.
- [64] S.J. Marshall, M. Balooch, S. Habelitz, G. Balooch, R. Gallagher, G.W. Marshall, The dentin - enamel junction - a natural, multilevel interface, *J. Eur. Ceram. Soc.* (2003), doi:[10.1016/S0955-2219\(03\)00301-7](https://doi.org/10.1016/S0955-2219(03)00301-7).
- [65] M.P. Walker, B. Fricke, Dentin-Enamel Junction of Human Teeth, *Wiley Encycl. Biomed. Eng.*, 2006, doi:[10.1002/9780471740360.ebs1431](https://doi.org/10.1002/9780471740360.ebs1431).
- [66] D. Shimizu, G.A. Macho, Functional significance of the microstructural detail of the primate dentino-enamel junction: a possible example of exaptation, *J. Hum. Evol.* (2007), doi:[10.1016/j.jhevol.2006.08.004](https://doi.org/10.1016/j.jhevol.2006.08.004).
- [67] D.S. Brauer, G.W. Marshall, S.J. Marshall, Variations in human DEJ scallop size with tooth type, *J. Dent.* (2010), doi:[10.1016/j.jdent.2010.03.010](https://doi.org/10.1016/j.jdent.2010.03.010).
- [68] Y. Li, C. Ortiz, M.C. Boyce, Stiffness and strength of suture joints in nature, *Phys. Rev. E* (2011), doi:[10.1103/PhysRevE.84.062904](https://doi.org/10.1103/PhysRevE.84.062904).
- [69] P.J. Motta, A quantitative analysis of ferric iron in butterflyfish teeth (Chaetodontidae, Perciformes) and the relationship to feeding ecology, *Can. J. Zool.* (1987) 65, doi:[10.1139/z87-016](https://doi.org/10.1139/z87-016).
- [70] N.H.C. Sparks, P.J. Motta, R.P. Shellis, V.J. Wade, S. Mann, An analytical electron microscopy study of iron-rich teeth from the butterflyfish (Chaetodon ornatissimus), *J. Exp. Biol.* (1990) 151, doi:[10.1242/jeb.151.1.371](https://doi.org/10.1242/jeb.151.1.371).
- [71] L.B. Whitenack, D.C. Simkins, P.J. Motta, Biology meets engineering: the structural mechanics of fossil and extant shark teeth, *J. Morphol.* 272 (2011), doi:[10.1002/jmor.10903](https://doi.org/10.1002/jmor.10903).
- [72] R.W. Thresher, G.E. Saito, The stress analysis of human teeth, *J. Biomech.* (1973), doi:[10.1016/0021-9290\(73\)90003-1](https://doi.org/10.1016/0021-9290(73)90003-1).
- [73] H. Chai, Dentin horn angle and enamel thickness interactively control tooth resilience and bite force, *Acta Biomater.* 75 (2018), doi:[10.1016/j.actbio.2018.06.001](https://doi.org/10.1016/j.actbio.2018.06.001).